The Astrophysical Journal, 646:801–814, 2006 August 1
© 2006. The American Astronomical Society. All rights reserved. Printed in U.S.A.

A SAMPLE OF LOW-REDSHIFT BL LACERTAE OBJECTS. II. EVN AND MERLIN DATA AND MULTIWAVELENGTH ANALYSIS

M. Giroletti,[1,2] G. Giovannini,[1,2] G. B. Taylor,[3,4] and R. Falomo[5]

Received 2005 December 19; accepted 2006 April 8

ABSTRACT

We present new radio observations of 9 members of a sample of 29 nearby ($z < 0.2$) BL Lac objects. The new data have been obtained with the European VLBI Network and/or MERLIN at 1.6 and 5 GHz and complement previous observations. For one object, the TeV source Mrk 421, we also present deep multiepoch VLBA and global VLBI data, which reveal a resolved diffuse jet with clear signatures of limb brightening. We use the new and old data to estimate physical parameters of the jets of the sample from which the subset with new radio data is drawn. We derive Doppler factors in the parsec-scale radio jet in the range $2 \lesssim \delta \lesssim 9$. Using *HST* data, we separate the contribution of the host galaxy from that of the active core. From the measured and debeamed observables, we find a weak correlation between radio power and black hole mass, and a tight correlation between radio and optical core luminosities. We interpret this result in terms of a common synchrotron origin, with little contribution from a radiatively efficient accretion disk. The BL Lac objects in our sample have debeamed properties similar to low-power radio galaxies, including the fundamental plane of black hole activity.

Subject headings: BL Lacertae objects: general — galaxies: active — galaxies: jets — galaxies: nuclei — radio continuum: galaxies

1. INTRODUCTION

In the unification schemes of radio-loud active galactic nuclei (AGNs), the reason for the difference between high-power (FR II radio galaxies and quasars) and low-power (FR I galaxies and BL Lacertae objects) sources is still a puzzling subject. In particular, it is not yet clear if it is related to evolutionary properties, to differences in the physical state of the central black hole (BH; see, e.g., Baum et al. 1995), and/or to a different interaction between the relativistic jet and the interstellar medium (De Young 1993).

In this context the study of BL Lac sources is important for many reasons. First, BL Lac objects are not well studied in the radio band, and their physical properties in this band are not yet well known. For instance, detailed VLBI studies on BL Lac objects are available only for the bright objects of the 1 Jy sample (Cassaro et al. 2002) and a few other outstanding sources (Giroletti et al. 2004b; Piner & Edwards 2004; Rector et al. 2003). In spite of this lack of high-resolution data, BL Lac objects are ideal targets to be observed with VLBI, since they are beamed objects and represent a good laboratory to look for evidence of the presence of relativistic jets in low-power radio sources (Denn et al. 2000).

In order to investigate this class of AGNs, we selected a sample of nearby BL Lac objects from the *Hubble Space Telescope* (*HST*) snapshot image survey (Urry et al. 2000; Scarpa et al. 2000). The sample is composed of 30 objects with redshift $z < 0.2$ (Giroletti et al. 2004a, hereafter Paper I). At these low redshifts, the *HST* separates the contribution of the central core and of the host galaxy; in the radio we can probe with VLBI the parsec-scale relativistic jet. Moreover, we can study low-power objects that are weak in the radio, with a spectral energy distribution (SED) peaking at high $\nu_{\rm peak}$ (HBLs); in the inverse Compton part of their SED, some members of the sample reach even the TeV domain. By contrast, their radio power is extremely low, which makes them comparable to radio-quiet objects when we consider their debeamed luminosity.

In Paper I, we presented Very Large Array (VLA) and Very Long Baseline Array (VLBA) observations for 15 objects. We have discussed some of the basic radio properties of the sample, and we have made a first estimate of the parsec-scale jet properties. In the present paper we present new observations of nine objects with the European VLBI Network (EVN) and MERLIN, including unpublished images of Mrk 421. Moreover, we take advantage of the data from the *HST* snapshot survey and from X-ray satellites in order to discuss the properties of the sample from a broadband perspective.

The paper is laid out as follows: § 2 contains a summary of the results of Paper I and introduces the new data sets; in § 3 we present the results of the new observations and details about individual sources; in § 4 we discuss the broadband properties of the sample; finally, § 5 summarizes the main conclusions of the present work. Throughout the paper, we use $H_0 = 70$ km s^{-1} Mpc^{-1}, $\Omega_M = 0.3$, and $\Omega_\Lambda = 0.7$. Spectral indexes are defined such that $S(\nu) \propto \nu^{-\alpha}$.

2. SAMPLE PROPERTIES AND NEW OBSERVATIONS

2.1. *The Sample: A Summary*

Based on the *HST* snapshot survey of BL Lac objects (Urry et al. 2000; Scarpa et al. 2000), we have selected a sample of 29 BL Lac objects with low redshift ($z < 0.2$). We point out that the sample considered in Paper I was composed of 30 sources. However, thanks to our analysis, we have been able to discard one object from the sample that is not a genuine BL Lac: we reject 0145+138 from the sample on the basis of its low core dominance ($S_c/S_t = 0.08$) and the lack of an unresolved nuclear component in the optical *HST* image. More observations and an optical spectrum would be desirable in order to understand its true nature. We also note that some objects (e.g., 0521−365, 2201+044) have

[1] INAF—Istituto di Radioastronomia, via Gobetti 101, 40129 Bologna, Italy; giroletti@ira.inaf.it, ggiovann@ira.inaf.it.
[2] Dipartimento di Astronomia, Università di Bologna, via Ranzani 1, 40127 Bologna, Italy.
[3] Department of Physics and Astronomy, University of New Mexico, Albuquerque, NM 87131; gbtaylor@unm.edu.
[4] National Radio Astronomy Observatory, P.O. Box O, Socorro, NM 87801.
[5] INAF—Osservatorio Astronomico di Padova, vicolo Osservatorio 5, 35122 Padova, Italy; falomo@pd.astro.it.

TABLE 1
OBJECTS IN THE SAMPLE

Name (IAU) (1)	Name (other) (2)	z (3)	$\log P_{1.4\ \mathrm{GHz}}$ (W Hz^{-1}) (4)	$-M_R$ (mag) (5)	$\log L_{2-10\ \mathrm{keV}}$ (erg s^{-1}) (6)	Ref. (7)	θ (deg) (8)	δ (9)	Class (10)	Sample (11)
0229+200		0.140	24.62	23.96	45.2	1	19	3.1	H	HEAO-A3
0347−121		0.188	24.32	22.56	45.0	2	23	2.6	H	HEAO-A3
0350−371		0.165	24.40	22.69	44.4	3	21	2.8	H	EMSS
0521−365		0.055	26.07	22.60	44.1	2	21	2.6	L	HEAO-A3
0548−322		0.069	24.72	23.05	44.6	2	32	1.9	H	HEAO-A2
0706+591		0.125	24.75	23.38	44.7	4	20	2.9	H	HEAO-A3
0806+524		0.137	24.90	22.87	45.3	1	14	4.1	H	Slew
0829+046		0.180	25.97	23.18	44.4	4	10	5.7	L	HEAO-A3
0927+500		0.188	24.26	22.50	45.3	1	16	3.5	H	Slew
1101+384	Mrk 421	0.031	24.27	22.57	45.0	2	19	3.0	H	HEAO-A3
1133+704	Mrk 180	0.046	24.17	22.24	43.7	2	24	2.5	H	HEAO-A3
1212+078		0.136	24.80	23.26	44.6	1	17	3.4	H	Slew
1215+303		0.130	25.36	23.15	43.7	2	15	3.7	H	Slew
1218+304		0.182	24.74	22.92	45.4	2	16	3.6	H	HEAO-A2
1229+643		0.164	24.59	23.43	44.8	3	17	3.3	H	EMSS
1255+244		0.141	23.88	22.67	45.1	2	24	2.5	H	Slew
1418+546	OQ 530	0.152	25.64	23.44	44.0	2	11	5.1	L	PG
1426+428		0.129	24.36	23.03	45.2	2	21	2.7	H	HEAO-A3
1440+122		0.162	24.62	23.04	45.1	1	18	3.3	H	Slew
1514−241	AP Lib	0.049	25.06	22.88	43.4	4	6	9.3	H	1 Jy
1652+398	Mrk 501	0.034	24.61	24.01	44.9	2	17	3.5	H	1 Jy
1728+502	I Zw 187	0.055	24.19	21.68	44.3	1	21	2.8	H	HEAO-A3
1807+698	3C 371	0.051	25.08	23.25	43.3	2	17	3.5	L	1 Jy
1959+650		0.048	24.12	22.46	44.8	2	17	3.4	H	HEAO-A3
2200+420	BL Lac	0.070	25.82	22.95	44.5	2	9	6.7	L	1 Jy
2201+044		0.027	24.12	21.86	42.9	4	29	2.1	L	HEAO-A3
2254+074		0.190	25.53	23.77	43.9	4	9	6.2	L	1 Jy
2344+514		0.044	24.24	23.53	44.2	2	21	2.8	H	Slew
2356−309		0.165	24.62	22.56	45.5	2	19	3.0	H	HEAO-A3

NOTES.— Col. (7): Reference for the X-ray luminosity. Col. (8): Uncertainty on the viewing angle θ is typically $\pm 5^\circ$ (but see discussion in § 4). Col. (10): H: High-frequency peaked BL Lac; L: low-frequency peaked BL Lac. Col. (11): 1 Jy (Stickel et al. 1991); HEAO-A2 (Piccinotti et al. 1982); HEAO-A3 (R. Remillard et al. 1999, private communication); EMSS (Morris et al. 1991); Slew (Schachter et al. 1993; Perlman et al. 1996).

REFERENCES.— (1) Perlman et al. 1996; (2) Donato et al. 2005; (3) Rector et al. 2000; (4) Donato et al. 2001.

optical spectra showing emission and absorption lines and are similar to Seyfert 1 spectra, but with lines of lower luminosity. In total, we have seven sources with a low-frequency synchrotron peak (LBLs) and 22 HBLs. The total radio powers span the range $10^{23.9}$–$10^{26.1}$ W Hz^{-1} at 1.4 GHz.

Table 1 shows in detail the list of objects in the sample and their basic properties, including the IAU name and other name in Columns (1) and (2), redshift in column (3), monochromatic power at 1.4 GHz from the NVSS in column (4), optical absolute magnitude in R band from the *HST* snapshot survey (Urry et al. 2000) in column (5), and X-ray luminosity in the 2–10 keV band in column (6) obtained from the *BeppoSAX* archive cataloged by Donato et al. (2005) or from other references as listed in column (7). Note that the radio and X-ray emission in BL Lac objects is variable; when more than one measurement was available in the *BeppoSAX* archive, we used the mean value. Columns (8) and (9) report the viewing angle θ and Doppler factor δ estimated on the basis of the arguments discussed in Paper I.[6] Finally, we report the object type in column (10) and the original sample in column (11).

In Paper I we presented radio images from parsec to kiloparsec scales for the whole sample, considering new and published VLA and VLBA observations. All objects are core dominated on kiloparsec scales; extended structure, however, is usually present, either symmetric or one-sided, in the form of jets, halos, and/or secondary compact components. On parsec scales we found weak cores and a few short, one-sided jets. The VLBA images account for most of the arcsecond core flux density, implying that we have not missed considerable subarcsecond structure. Parsec- and kiloparsec-scale jets are oriented at the same position angle (P.A.) in a large fraction of objects, in contrast with the large bending angles found in several BL Lac objects of the 1 Jy sample (ΔP.A. $> 90^\circ$; Cassaro et al. 2002). If large bends are ascribed to geometric amplification of small oscillations in jets closely aligned to the line of sight, the similarity in the P.A. of the parsec- and kiloparsec-scale jets found in our sample implies that their viewing angles are larger than those of the LBLs in the 1 Jy sample (see also Rector et al. 2003). From the jet/counterjet ratio, the synchrotron self-Compton (SSC) model, and primarily from the core dominance, we estimate the range of possible parameters of the jets. Under the statistical assumption of $\Gamma \sim 1/\sin\theta$, we derived an average viewing angle of $\langle\theta\rangle = 18^\circ \pm 5^\circ$ and Lorentz factors Γ of the jets in the range $2 \lesssim \Gamma \lesssim 9$.

The properties of the host galaxies have been presented by Falomo et al. (2000) based on the original *HST* data for the sample. The hosts are virtually all massive elliptical galaxies (average luminosity $M_R = -22.9 \pm 0.6$ and effective radius $R_e = 10$ kpc), typically located in poor groups. In spite of the presence of the

[6] In Paper I we only listed values assuming $\Gamma = 5$. The data shown in cols. (8) and (9) are derived in the case that $\Gamma \sim 1/\theta$ and they can then be different from those found in our earlier work.

TABLE 2
Log of Observations Considered in This Paper

Date (1)	Array (2)	Frequency (GHz) (3)	Sources (4)
2002 Jun 7	E	1.6	0706+591, 0806+524, 1133+704, 1215+303, 1218+304, 1229+643, 1426+428, 1728+502
2002 May 26	E, M, EM	5	1215+303, 1728+502
1997 Feb 17	E, M, EM	5	1101+384
1996 Feb 10	G	1.6	1101+384
1995 Jul 22	V	5	1101+384

Notes.—Col. (2): E = EVN; M = MERLIN; EM = EVN+MERLIN; G = Global VLBI; V = VLBA + Y1 (see text for details).

active nucleus, the host galaxy appears in most cases to be a completely "normal" elliptical galaxy. Moreover, the data have shown that no significant difference is present between the hosts of HBLs and those of LBLs.

2.2. *Observations and Data Reduction*

In this paper we present new radio observations of nine BL Lac objects. We list the various data sets at our disposal in Table 2. For eight sources (i.e., all except 1101+384), we have EVN observations at 1.6 GHz in single polarization taken on 2002 June 7. The stations involved were Effelsberg (100 m), Jodrell Bank (Mk II, 25 m), Medicina (32 m), Noto (32 m), Onsala (25 m), Sheshan (25 m), Torun (32 m), Westerbork (14×25 m), and Urumqi (25 m). Each source was observed for $\sim$55 minutes, divided into four scans at different hour angles to obtain good u-v coverage. The data were correlated at the Joint Institute for VLBI in Europe (JIVE) in Dwingeloo. We imported the data in the National Radio Astronomy Observatory (NRAO) Astronomical Image Processing System (AIPS) and performed the a priori calibration. Finally, we edited the data and produced the images within DIFMAP; the final restoring beams, 3 σ noise levels, and image peaks are reported in Table 3.

Two of the sources (1215+303 and 1728+502) were also observed at 5 GHz with the EVN and the MERLIN simultaneously on 2002 May 26. The EVN array involved in the experiment includes the same telescopes of the EVN-only observation, plus the 32 m antenna in Cambridge; this antenna provides a baseline to Jodrell Bank, common to the MERLIN array as well. Each source was observed for 6 hr, in 42 scans, switching between the two targets. The MERLIN data have been processed at Jodrell Bank Observatory with the local `dprograms`; DIFMAP has been used to produce the images. The EVN data were correlated in Dwingeloo and reduced in the standard manner within AIPS (for initial calibration) and DIFMAP (for the imaging part). Finally, the combination of the two data sets has been done within AIPS, using the task `DBCON`. For the combined data set, we have modified the weights of the original data in order to optimize the compromise between resolution and sensitivity by means of the adverb `REWEIGHT` in `DBCON`; in particular, the EVN data have been rescaled by a factor of 20.

Moreover, we present here unpublished data for 1101+384 (Mrk 421): (1) EVN+MERLIN observations taken on 1997 February 17 at 5 GHz (the EVN telescopes involved in the observation were Effelsberg, Sheshan, Cambridge, Medicina, Torun, and the VLBA dish in Saint Croix; the MERLIN array consisted of Defford, Cambridge, Knockin, Darnall, Mk II at Jodrell Bank, and Tabley; we have about 6 hr of EVN observations and three hours with the MERLIN after flagging for down time, bad weather, and receiver problems; we followed the procedures outlined above for the data reduction of the EVN and MERLIN data set and for their combination); (2) observations with the VLBA plus a single VLA dish (VLBA+Y1) for 4 hr at 5 GHz on 1995 July 22; (3) observations at 1.6 GHz on 1996 February 10 with a global array (six VLBA telescopes for 6 hr, including 3 hr at Jodrell Bank, Medicina, Noto, and Onsala). A preliminary map based on this observation was presented by Giovannini et al. (1999). See Table 4 for the restoring beam, peak and noise level of all our new images of Mrk 421.

3. RESULTS

3.1. *General Properties*

We show in Figure 1 the milliarcsecond-scale images of the eight BL Lac objects observed at 1.6 GHz with the EVN; we report their relevant parameters in Table 3. Typically, the sources are dominated by a compact core making up the largest fraction of the total flux density. Jets are detected in seven out of eight

TABLE 3
EVN Observations at 1.6 GHz, Image Parameters

Name	HPBW (mas × mas, deg)	Noise (3 σ) (mJy beam^{-1})	Peak (mJy beam^{-1})
0706+591	$8.8 \times 6.9, -55$	0.5	33.5
0806+524	$10.9 \times 4.3, -26$	2.0	98.0
1133+704	$5.1 \times 4.5, -28$	3.0	67.2
1215+303	$12.5 \times 4.1, 7$	1.0	224.5
1218+304	$12.5 \times 4.2, 6$	1.0	48.7
1229+643	$10.0 \times 4.6, 7$	1.3	44.1
1426+428	$8.8 \times 4.3, 3$	1.4	28.8
1728+502	$12.1 \times 5.5, -58$	1.0	107.4

TABLE 4
EVN+MERLIN Observations at 5 GHz, Image Parameters

Source	Array	HPBW (mas × mas, deg)	Noise (3 σ) (mJy beam^{-1})	Peak (mJy beam^{-1})
1215+303	MERLIN	$55 \times 52, 29$	0.35	315
	EVN+MERLIN	$11.7 \times 8.2, 12$	0.40	294
	EVN	$5.2 \times 1.9, 7$	0.38	274
1728+502	MERLIN	$51 \times 47, -31$	0.40	163
	EVN+MERLIN	$7.6 \times 6.4, 38$	0.27	116
	EVN	$2.2 \times 1.6, 15$	0.43	92
Mrk 421	MERLIN	$79 \times 47, 11$	1.2	530
	EVN+MERLIN	$11.4 \times 9.8, 43$	0.87	426
	EVN	$6.5 \times 3.1, -9$	0.65	407
	VLBA+Y1	$3.6 \times 2.6, -19$	0.64	338
	Global VLBI	$7.0 \times 3.9, 8$	1.2	332

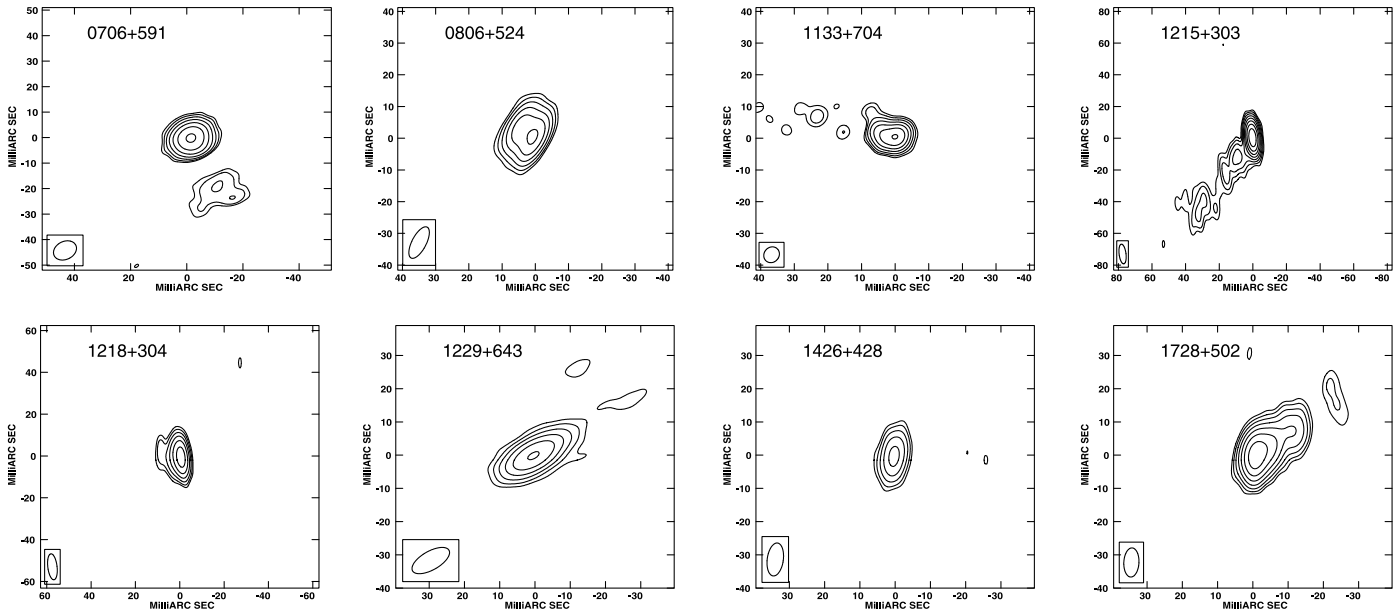


FIG. 1.— EVN images taken at 1.6 GHz on 2002 June 7. Contours are drawn at (1, 2, 4, 8, 16, . . .) times the noise level. Noise levels and image peaks are given in Table 3.

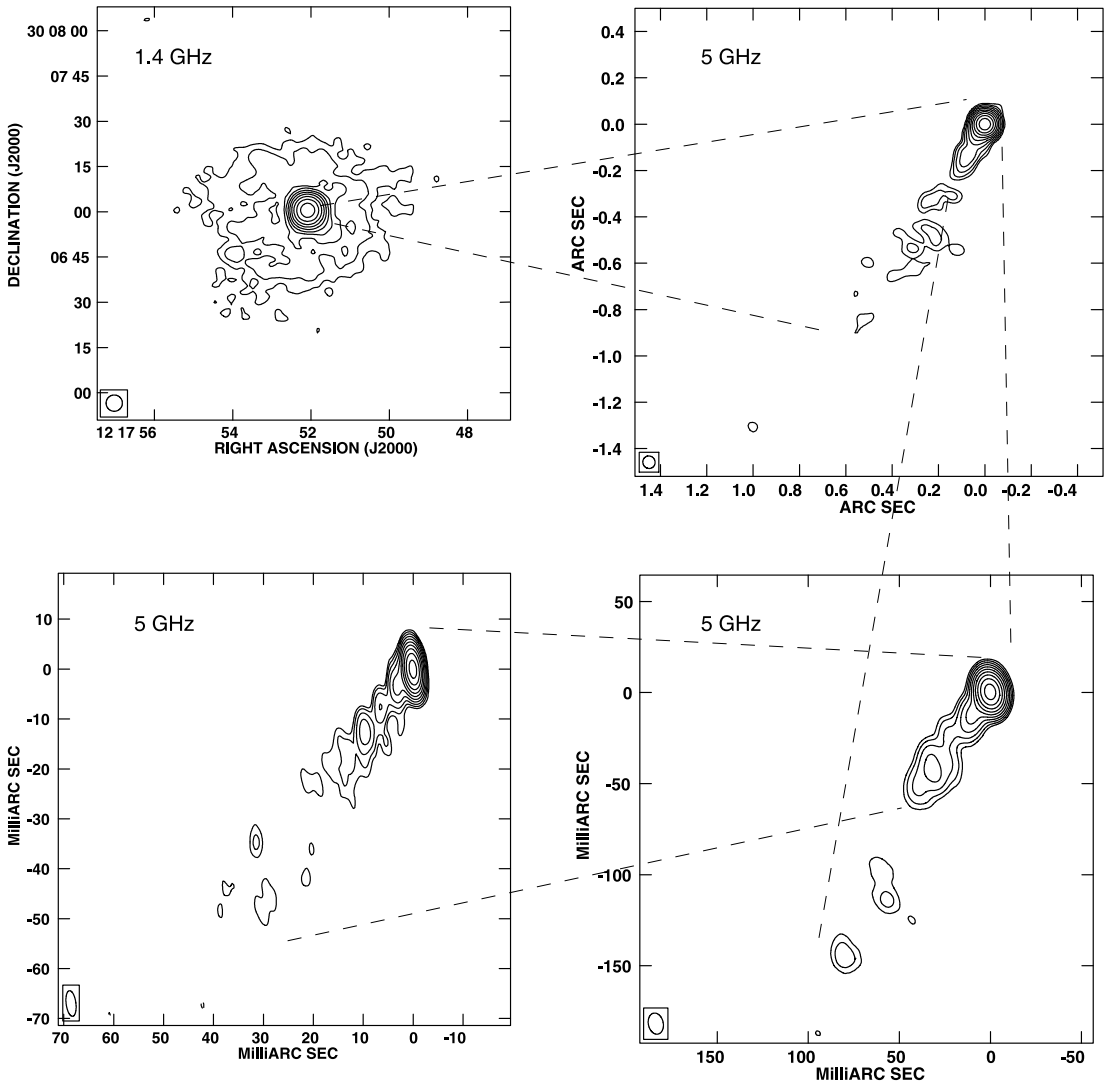


FIG. 2.— Images of 1215+303. *Clockwise from top left*: FIRST, MERLIN, EVN+MERLIN, and EVN-only images. Contours are traced at (−1, 1, 2, 4, . . .) times the noise levels. Beam, noise, and peak for the EVN and MERLIN images are given in Table 4; the noise in the FIRST image is 0.45 mJy beam^{-1}.

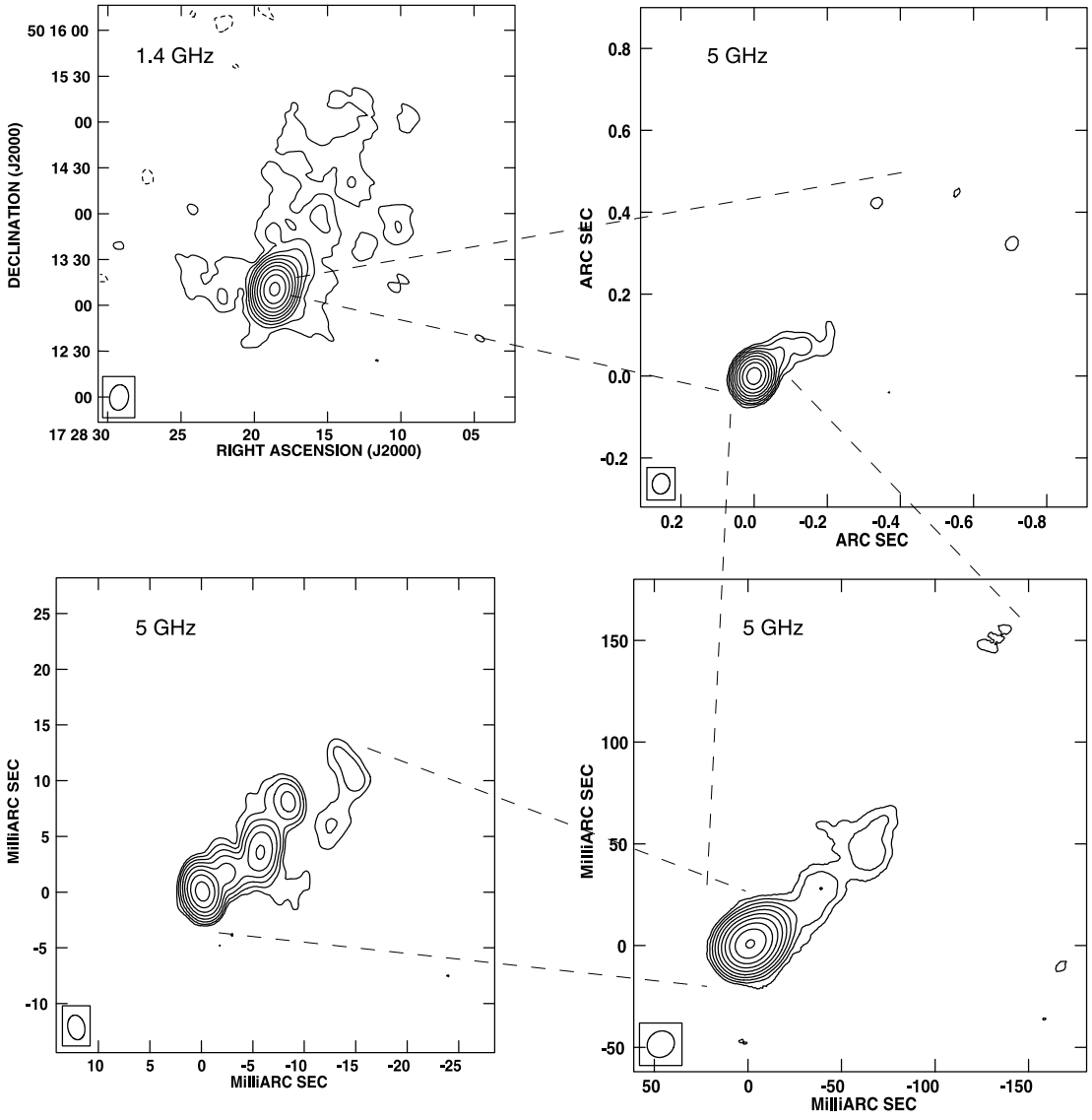


FIG. 3.— Images of 1728+502. *Clockwise from top left*: VLA, MERLIN, EVN+MERLIN, and EVN-only images. Contours are traced at (−1, 1, 2, 4, . . .) times the noise levels. Beam, noise, and peak for the EVN and MERLIN images are given in Table 4; the noise in the VLA image is 0.3 mJy beam^{-1} (see Paper I).

sources, always single sided. This rate of jet detection (83%) is higher than in the 5 GHz VLBA observations of other objects of the sample (8/15, or 53%; see Paper I). This may stem from both the longer exposure and brighter targets of the present observations.

We also present several deep radio images at 5 GHz for 1215+303 (Fig. 2) and 1728+502 (Fig. 3), and at 1.6 and 5 GHz for 1101+ 384 (Mrk 421; Figs. 4 and 5). These images span scales from a few parsecs to some kiloparsecs and include our new EVN+MERLIN combination. These sources possess bright cores and longer (>100 mas) one-sided jets. The jets are remarkably well aligned on scales from a few to some hundreds of parsecs (projected). Evidence of bending is present only in the inner parsecs of the jet of Mrk 421. We provide more details on these sources in §§ 3.2 and 3.3, including a description of their kiloparsec-scale properties.

In Table 5, we report the results of our model fits to the visibility data for the EVN 1.6 GHz observations. In column (1) we give the source name, in column (2) the various components studied for each source, and in columns (3)–(6) the details of the model for that component: flux density, radius r (i.e., distance from an arbitrary origin), position angle θ, and FWHM b. These models have been obtained fitting circular Gaussian components to the data using `modelfit` in DIFMAP. We adopt circular Gaussians because the signal-to-noise ratio (S/N) is relatively low in most jets, and we need to keep the number of parameters as low as possible. The models for the most compact and powerful components are typically better constrained than for weak and extended ones, although the various model parameters are not independent of each other. Typically, components smaller than 10 mas have uncertainties on r and b of $\sim$0.5 mas or less. For larger components, uncertainties are estimated on the basis of the half-power beamwidth (HPBW) of the image and the component SNR. For the flux densities, we estimate the uncertainty from the rms noise and the absolute flux calibration uncertainty ($\sim$10%) added in quadrature. We then summarize in Table 6 the main results about cores and jets properties, based on the new 1.6 and 5 GHz EVN data, as well as on the 5 GHz VLBA data presented in Paper I. We give the core flux density at 1.6 GHz in column (2), and the one at 5 GHz in column (3), either using present EVN data or the VLBA data in Paper I. The corresponding nonsimultaneous spectral index is given in column (4). Columns (5) and (6) contain the jet brightness B_j and the relative lower limit on the jet/counterjet ratio $R_{\rm min}$.

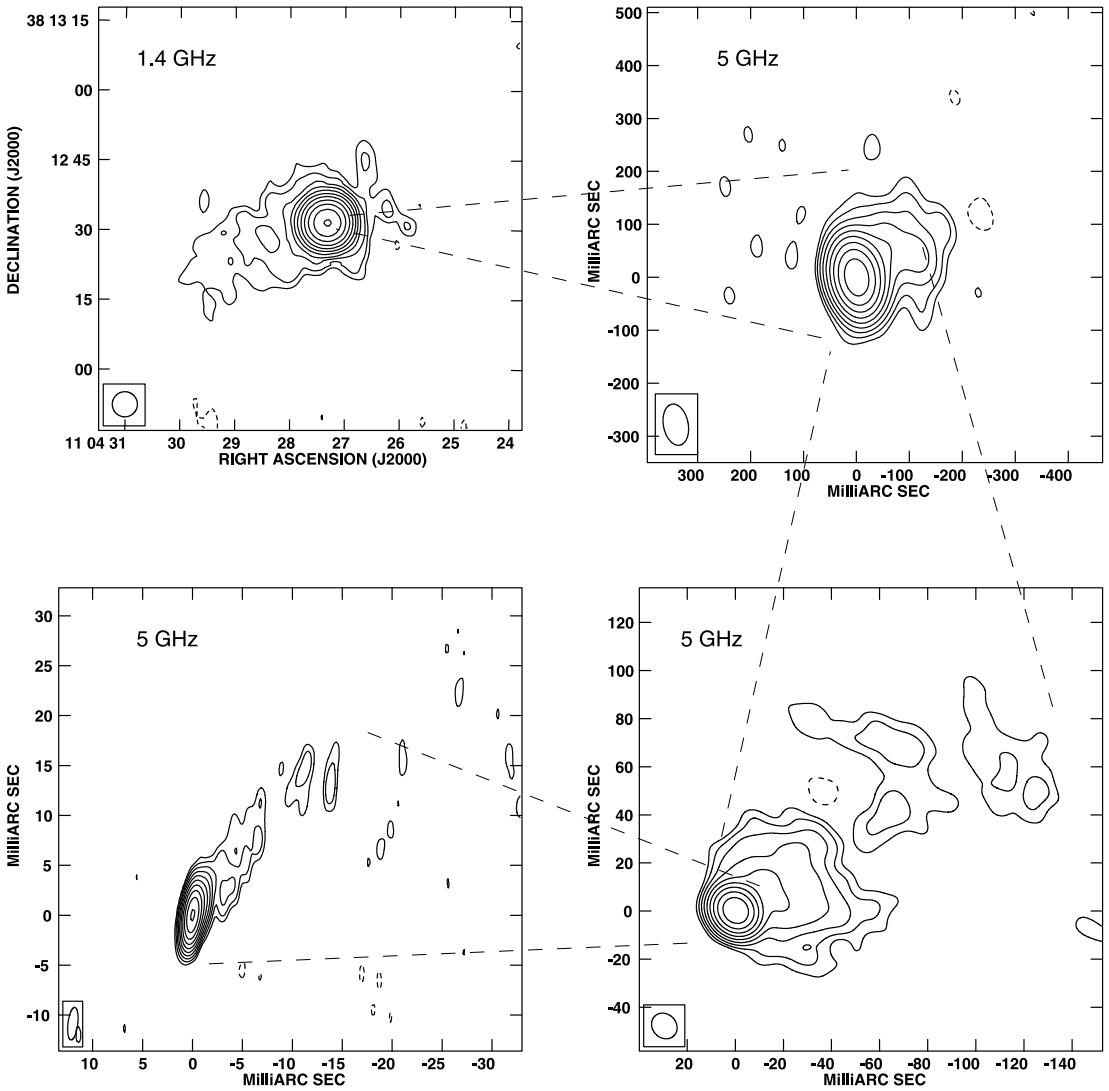


FIG. 4.— Images of Mrk 421. *Clockwise from top left*: FIRST, MERLIN, EVN+MERLIN, and EVN-only images. Contours are traced at $(-1, 1, 2, 4, \ldots)$ times the noise levels. Beam, noise, and peak for the EVN and MERLIN images are given in Table 4; the noise in the FIRST image is 0.5 mJy beam^{-1}.

Core flux densities have been derived from the fits of Gaussian components to the data. The core flux density is expected to be slightly higher than the peak brightnesses of the images reported in Table 3 because of the discrete map gridding. In a few cases (1133+704, and 1215+303), the significantly larger core flux density indicates that there is some contamination from the jet. At full resolution, the different observing frequency brings about an excess of flux density in the 1.6 GHz data, mostly as a result of the different size of the synthesized beams. For a spectral index measurement, we therefore consider our 5 GHz images (either VLBA or EVN), limiting the u-v range to 0–40 Mλ; this yields a resolution comparable to the 1.6 GHz images. Results are presented in Table 6, with $\alpha^{5}_{1.6}$ in the range between -0.1 and 0.5. Note that the observations at 1.6 and 5 GHz are not simultaneous, so variability can account for part of the differences.

All the sources display single-sided jets in both 1.6 and 5 GHz data, except for 1426+428, which has a tentative jet detection only at 5 GHz (Kollgaard et al. 1996). In most cases we need only one component (in addition to the core) to model-fit the jet. We also measured flux densities and brightnesses directly on the images. Since no object in the sample has a detectable counterjet, the brightness ratios presented in Table 6 are only lower limits based on the noise of the images. More details are given along with the source description in the next section.

For 1215+303, 1728+502, and Mrk 421 we have also obtained spectral index maps (simultaneous in the case of 1215+303 and 1728+502). Cores are typically flat/inverted, while the jets are steeper in general. However, the S/N is too low to make any strong statement about possible substructures within the jet and we do not show these images here.

3.2. *Notes on Single Sources*

0706+591.—The EVN jet points at approximately -150°. A significant fraction of flux density (about 14%) is found in a component at $\sim$17 mas ($\sim$40 pc) from the core, with a peak brightness of 2.0 mJy beam^{-1}. The comparison with VLA and VLBA images in Paper I (see also Giroletti et al. 2005) confirms the orientation of the parsec-scale jet and its misalignment to the kiloparsec-scale extended structure. The core sits at the northwest edge of a diffuse extended halo, with major axis oriented at P.A. $\sim 120^{\circ}$.

0806+524.—The EVN observation at 1.6 GHz recovers a total of 181 mJy. This source is then one of the most core dominated in the sample ($S_{\rm NVSS} = 183$ mJy). A well-defined jet component is

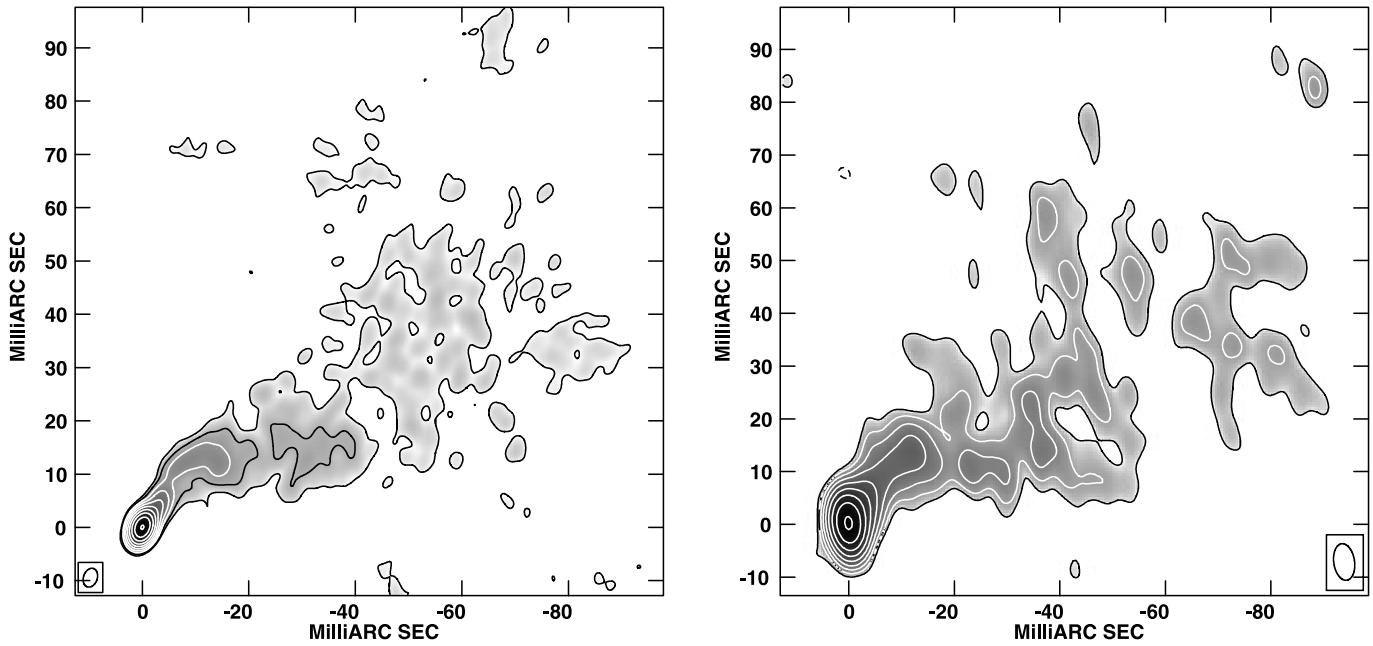


FIG. 5.—Images of Mrk 421. *Left*: VLBA+Y1 at 5 GHz (epoch 1995.7); *right*: global VLBI at 1.6 GHz (epoch 1996.2). Contours are traced at (−1, 1, 2, 4, ...) times the noise levels. Beam, noise, and peak are given in Table 4.

found at 4.8 mas from the core at P.A. = 42°, i.e., only slightly misaligned (ΔP.A. $\sim$ 35°) with respect to the VLBA jet at 5 GHz (Paper I).

1101+384 (Mrk 421).—See § 3.3.

1133+704.—Our data reveal a short inner jet (P.A.$_j \sim 70°$) and some more distant low-brightness emission. Both features are well aligned with the major axis of the kiloparsec-scale halo shown in Paper I, as well as the parsec-scale jet found by Kollgaard et al. (1996).

TABLE 5
RESULTS OF THE MODEL FITS TO THE EVN 1.6 GHz OBSERVATIONS

Source (1)	Component (2)	Flux Density (mJy) (3)	r (mas) (4)	θ (deg) (5)	b (mas) (6)
0706+591	Core	36 ± 4	Ref.	Ref.	≤2.5
	J1	7 ± 1	16.8	−151	11 ± 2
0806+524	Core	97 ± 10	Ref.	Ref.	≤1.8
	J1	84 ± 9	4.8	42	3.1 ± 0.5
1133+704	Core	82 ± 8	Ref.	Ref.	≤1.8
	J2	36 ± 5	6.1	69	9.3 ± 1.5
	J1	9 ± 3	33.5	76	14 ± 3
1215+303	Core	261 ± 26	Ref.	Ref.	≤2.2
	J2	33 ± 3	18.4	143	9.8 ± 1.0
	J1	25 ± 3	52.7	145	16 ± 2
1218+304	Core	49 ± 5	Ref.	Ref.	≤1.7
	J1	15 ± 2	5.2	84	4.3 ± 1.3
1229+643	Core	48 ± 5	Ref.	Ref.	≤2.1
	J1	15 ± 2	23.9	−50	32 ± 10
1426+428	Core	32 ± 4	Ref.	Ref.	≤1.9
1728+502	Core	110 ± 11	Ref.	Ref.	≤2.1
	J2	76 ± 8	7.1	−49	3.6 ± 0.5
	J1	11 ± 2	21.3	−55	6.6 ± 1.5

NOTES.— Results of circular Gaussian model fits to the EVN 1.6 GHz visibility data. Col. (2): jet components are numbered J1 and J2 from the outermost inward. Cols. (4), (5), and (6): r, θ, b = radius, P.A., and FWHM of the component. See § 3 for a discussion of uncertainties.

1215+303.—The HBL 1215+303 is located at $z = 0.130$. For this object, a good map is available in the FIRST survey (Becker et al. 1995), as shown in Figure 2 (*top left*). A 377 mJy core dominates a symmetric halo structure of about 50″ diameter. No preferred direction is visible on this scale, while the EVN 1.6 GHz image shows a jet oriented at P.A. = 140°. For this reason, we consider also the EVN+MERLIN observations at 5 GHz in order to image the inner structure out to the largest possible distance from the inner core. The other panels in Figure 2 show the long, straight, one-sided jet. The large jet/counterjet ratio ($R \gtrsim 150$) indicates that the effects of the beaming are important in this source; indeed, one could expect a small angle to the line of sight if the kiloparsec halo structure were interpreted as a lobe seen end-on.

1218+304.—The total VLBI correlated flux at 1.6 GHz is 64 mJy, and it dominates the total flux density of the source ($S_{\rm NVSS}$ = 71.3 mJy). The core spectral index is $\alpha = 0.1$; a weak jet at P.A. = 84° is present at both 1.6 and 5 GHz (see Paper I).

TABLE 6
CORE AND JET OBSERVATIONAL PROPERTIES

Source (1)	$S_{c,1.6\rm GHz}$ (mJy) (2)	$S_{c,5\rm GHz}$ (mJy) (3)	Spectral Index (4)	B_j (mJy beam^{-1}) (5)	$R_{\rm min}$ (6)
0706+591	36	36	0.0	2.0	12
0806+524	97	100	−0.0	69.5	108
1101+384	325	323	0.0	22.0	110
1133+704	82	83	−0.0	32.0	33
1215+303	261	292	−0.1	9.4	150
1218+304	49	43	0.1	6.0	18
1229+643	48	26	0.5	2.0	5
1426+428	32	19	0.5	...	...
1728+502	110	117	−0.1	18.0	200

NOTES.—Core flux densities and spectral indexes are calculated considering only u-v data in the range 0–40 Mλ. The 5 GHz data are taken from Paper I, except for 1215+303 and 1728+502 (EVN; present work) and 1133+704 and 1426+428 (EVN; Kollgaard et al. 1996). Flux densities at 1.6 GHz are from EVN 2002 data, except for 1101+384, which is from the global VLBI experiment of 1996.

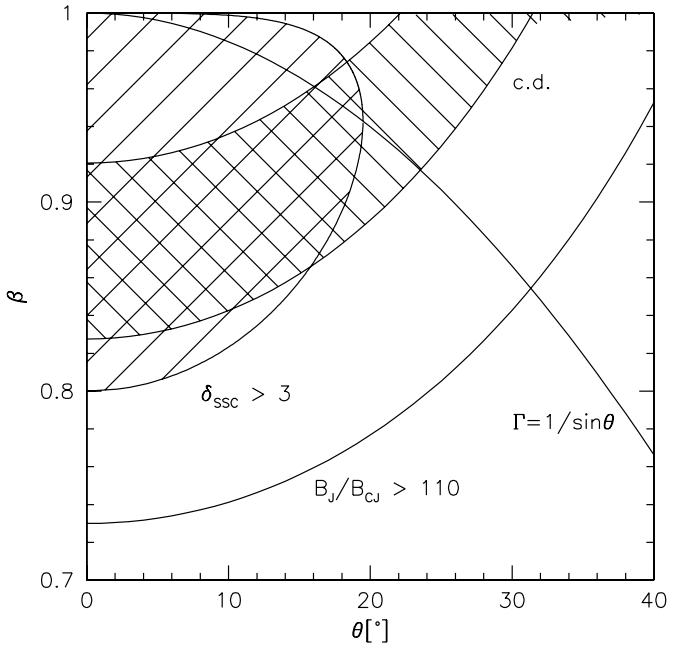


FIG. 6.—Plane (β, θ) for the jet of Mrk 421, with constraints derived from jet/counterjet ratio, core dominance (c.d.), and the SSC model. The cross-hatched area represents the (β, θ) pairs that satisfy the observational data. The relation $\Gamma = 1/\sin\theta$ is also shown; its section within the hatched area corresponds to the most likely combinations of jet velocity and orientation.

1229+643.—The 5 GHz VLBA image (Paper I) clearly shows a core-jet structure at P.A. $= -43^\circ$. In the present 1.6 GHz image, most of this emission is blended in the core component. Little flux density is detected in the same position angle at a larger distance. The total flux density recovered by the EVN is 61 mJy and exceeds that of the kiloparsec-scale core (55 mJy; Paper I), calling for significant variability in this source.

1426+428.—This BL Lac is a TeV source (Aharonian et al. 2002; Horan et al. 2002). It is unresolved in our EVN image, with a total flux density of 32 mJy. This makes up about 50% of the total flux density at 1.4 GHz in the NVSS (61 mJy).

1728+502.—This source displays a remarkable alignment from the parsec-scale EVN image out to the NVSS map, going by our new MERLIN and earlier VLA (Giroletti et al. 2004a) observations (see Fig. 3). The parsec-scale jet at P.A. $= -55^\circ$ is still collimated on the MERLIN scale, with a little tilt east. Then, in the C-array VLA image, the emission is spread over more than $100''$, for a total of $\sim$16 mJy of extended emission. This emission is resolved in the A-array image, which is dominated by the 200 mJy core.

3.3. *Markarian 421*

Mrk 421 ($z = 0.031$; 1 kpc $= 0''.6$) is a well-known BL Lac, widely studied at all frequencies and detected at TeV energies (Punch et al. 1992). The NVSS image shows a $30''$ core-dominated source, with emission on either side. As we increase the resolving power of our images and get closer to the core region, more and more extended emission becomes resolved out and finer details are discovered. In Figure 4, we see the dominant structure shift from the eastern side (FIRST image; *top left*) to the west (MERLIN and EVN images; *clockwise from top right*). The parsec-scale data (see also Fig. 5) convincingly show that the approaching side is the western one. On the basis of the parsec-scale observational data, we estimate that the viewing angle is $\theta \lesssim 20^\circ$. In Figure 6 we combine the constraints posed by the jet-counterjet ratio ($R > 110$ at 13 mas from the core), core dominance, and synchrotron self-Compton excess, $\delta_{SSC} \gtrsim 3$, based on a VLBI core of $\sim$300 mJy and an upper limit to the angular diameter of 0.1 mas. We estimate an orientation for the radio jet of $\theta = 18^\circ \pm 2^\circ$ under the assumption of $\Gamma \sim 1/\sin\theta$. This corresponds to the maximum angle allowed for a given Doppler factor, which, in a statistical sense, is the most likely situation. Such a relatively large angle for a TeV radio source may indicate that this assumption could be inaccurate for Mrk 421, although it could also be suggestive of a change in the inner jet orientation, similarly to what is found in Mrk 501 (Giroletti et al. 2004b), as well as of the presence of a structured jet (see also Ghisellini et al. 2005).

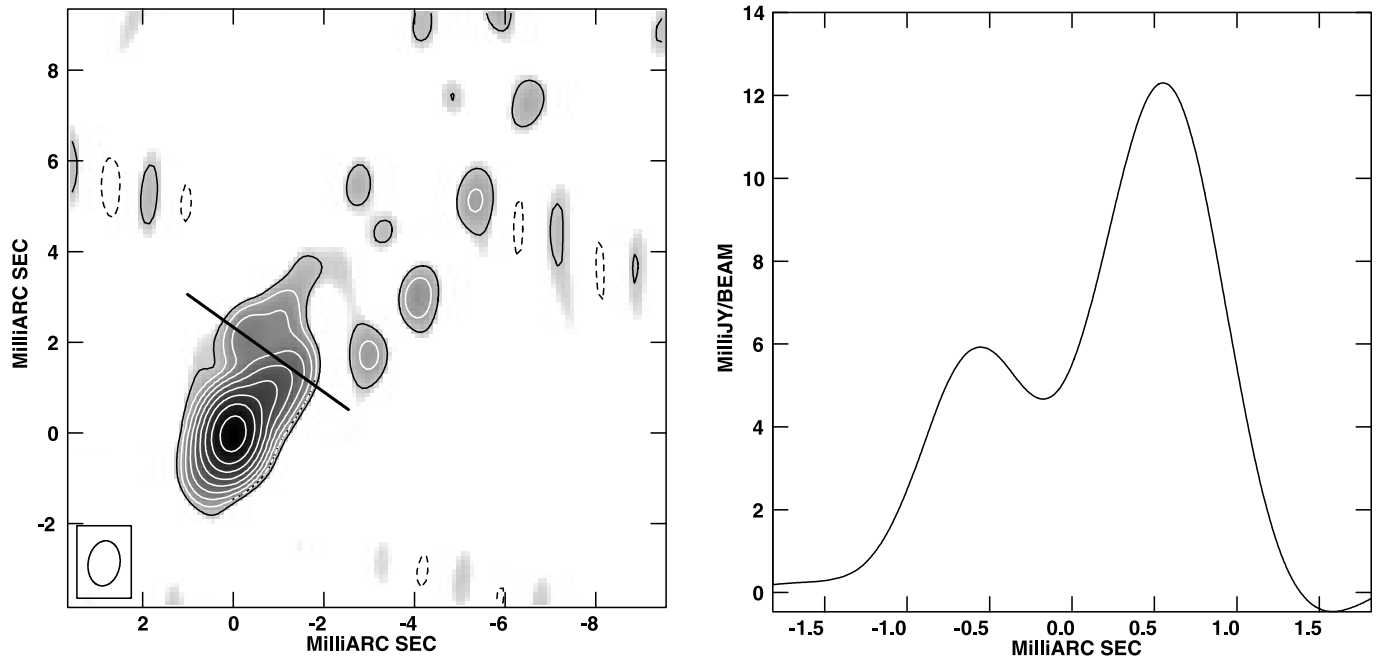


FIG. 7.—*Left*: High-resolution (beam 1.0×0.7 mas at P.A. $= -9^\circ$) image of the inner jet of Mrk 421 at 5 GHz with EVN, contoured at $(-1, 1, 2, 4, \ldots) \times 0.86$ mJy beam^{-1}. *Right*: Brightness profile along the slice shown in the left panel.

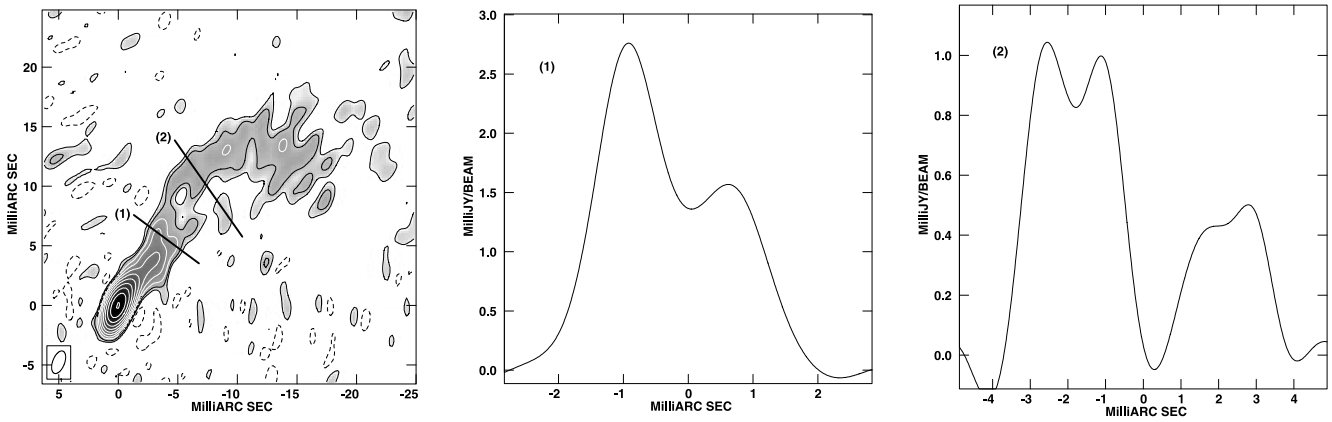


FIG. 8.—*Left*: High-resolution (beam 2×1 mas at P.A. $= -21^\circ$) image of the inner jet of Mrk 421 at 5 GHz with VLBA+Y1, contoured at $(-1,\ 1,\ 2,\ 4,\ \ldots) \times 0.3$ mJy beam^{-1}; the brightness profiles along the slices are shown in the center and right panels.

The jet of Mrk 421 is bright and well-collimated in the inner $\sim$20 mas, and it then becomes fainter and wider, with an opening angle $\phi_o \sim 40^\circ$. Under the viewing angle of 18°, this corresponds to an intrinsic jet opening angle $\phi_i \sim 12^\circ$. The jet shows also some bending from P.A. $= -35^\circ$ close to the core to P.A. $= -65^\circ$ at a larger distance. Both the change in collimation and the bending—although less conspicuous—remind us of the other TeV BL Lac Mrk 501, whose parsec-scale jet turns by 55° and widens significantly at about 30 mas from the core. Giroletti et al. (2004b) have studied the jet of Mrk 501, discussing also evidence of limb brightening in the inner 30 mas.

Although less prominent, an enhanced brightness at the jet edge is visible also in our images of Mrk 421. In Figure 7 we show a high-resolution image obtained from the 1997 EVN data with uniform weights: the jet is clearly transversally resolved at $\sim$2 mas from the core (see also Piner & Edwards 2005). Thanks to the 1995 VLBA+Y1 5 GHz observation, we extend this study and consider a more distant region, at $\sim$10–15 mas, which is illustrated in Figure 8. The gray-scale image and the brightness profiles across the jet reveal a clear limb-brightening, which is most prominent on the northeast side. After the bend, the jet is well resolved and it is clearly not centrally peaked; a possible limb-brightening could also be present at about 30 mas from the core on the right edge of the jet, as visible in Figure 5 both at 1.6 and 5 GHz.

If we interpret the brightness morphology as a velocity structure in the jet, we have an agreement with observational data if $\theta = 18^\circ$ assuming a fast spine structure ($\Gamma_{\rm spine} = 10$–15, corresponding to $\delta = 1.9$–1.3) and a slower external sheath ($\Gamma_{\rm sheath} = 2$–5, corresponding to $\delta = 2.9$). The larger δ in the slower sheath will thus account for the observed brightness structure.

As is the case also in Mrk 501, the resolved and limb brightened structure of the jet makes it difficult to describe the jet with simple Gaussian components. We have nonetheless tried to model-fit the data with circular Gaussians, and we find that the inner jet is well described by a core plus three components (see Table 7), in good agreement with results at higher frequency of Piner & Edwards (2005). In particular, we match our two innermost components with their C4 and C5. However, given the larger number of epochs considered by Piner & Edwards (2005), our data do not improve over their study of the motion of component, which we regard as conclusive. The small observed velocities [peak velocity of $(0.1 \pm 0.02)c$] confirm also our results on the similar source Mrk 501 (Giroletti et al. 2004b): low-power radio sources with complex, limb-brightened jets show low $\beta_{\rm pattern}$, which is therefore not related the bulk velocity of the jet.

4. DISCUSSION

Thanks to the new data presented here and in Paper I, we estimate the relevance of beaming in our sample of nearby BL Lac objects. As discussed in Paper I, we base our estimates for the jet parameters on (1) the jet-counterjet brightness ratio; (2) the core enhancement with respect to the value expected from the low-frequency, not-boosted total radio power; (3) the measured 1 keV flux densities with respect to the SSC predicted ones. In particular, the core dominance selects a region of the space of parameters

TABLE 7
RESULTS OF THE MODEL FITS TO MARKARIAN 421

Epoch (1)	Component (2)	Flux Density (mJy) (3)	r (mas) (4)	θ (deg) (5)	b (mas) (6)
1995.56.....	Core	335 ± 34	Ref.	Ref.	≤ 0.4
	C5	25 ± 3	1.8	-32	≤ 0.4
	C4	15 ± 2	4.7	-38	1.6 ± 0.5
	C3	81 ± 8	27.6	-56	38 ± 15
1996.11.....	Core	232 ± 23	Ref.	Ref.	≤ 0.4
	C5	105 ± 11	1.3	-40	≤ 0.4
	C4	43 ± 5	5.1	-39	3.0 ± 0.7
	C3	219 ± 22	26.2	-55	48 ± 15
1997.13.....	Core	398 ± 40	Ref.	Ref.	≤ 0.4
	C5	24 ± 3	1.4	-42	≤ 0.4
	C4	19 ± 2	5.7	-36	1.3 ± 0.5
	C3	17 ± 2	16.4	-39	10 ± 5

NOTES.—Results of circular Gaussian model fits to the visibility data of Mrk 421. C5 and C4 are labeled following Piner & Edwards (2005); the more extended C3 is resolved in their high-frequency observations and is also poorly constrained in our models. Cols. (4), (5), and (6): r, θ, and b = radius, P.A., and FWHM of the component. Uncertainty on r is typically 0.2 mas for C5 and 0.5 mas for C4.

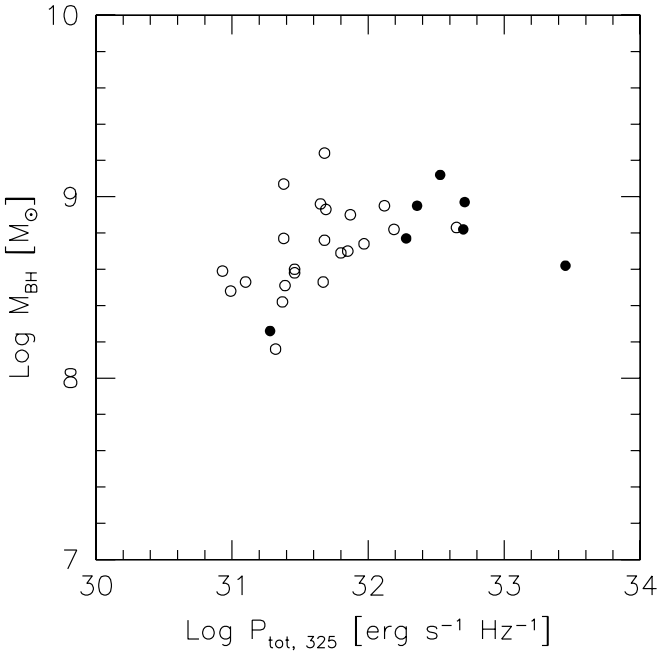


FIG. 9.—BH mass vs. total radio power at 325 MHz. Filled and open symbols represent HBL and LBL, respectively.

(β, θ), which can be either fully consistent or slightly restricted by the limits posed by (1) and (3). From this allowed region of the space of parameters, we derive the Lorentz factor Γ and the viewing angle θ, under the assumption that $\Gamma \sim 1/\sin\theta$. We note that for any one source the relation may not hold, although in a statistical sense this shall be the most likely solution.

With this caveat in mind, we derive the intrinsic properties of the sources in our sample. In this way, we are able to discuss their physical properties and address the issue of the parent population. For example, we have shown in Paper I that the debeamed nuclear radio luminosity are indistinguishable from those of a sample of FR I radio galaxies, in addition to what is already well known about the extended radio luminosity. We will now adopt a broadband perspective and consider multiwavelength data, which provide a tool to investigate the mechanisms involved in the nuclear activity. For the present sample, a wealth of information is available thanks to the optical observations performed with the *Hubble Space Telescope*. In particular, for all the objects it has been possible to separate the contribution of a central compact core and of the host galaxy. Both quantities have significant impact on our understanding of the BL Lac phenomenon. The central compact core is a clear signature of the nuclear activity; the host galaxy luminosity is a tool to estimate the mass of the central black hole (Magorrian et al. 1998; Kormendy & Gebhardt 2001).

4.1. *BH Mass and Radio Power*

In the following, we adopt black hole mass estimates based on the host galaxies bulge luminosity. As discussed by Falomo et al. (2003), this method is preferable to those based on the correlation with the central stellar velocity dispersion σ (Ferrarese & Merritt 2000; Gebhardt et al. 2000). In fact, (1) direct measurements of σ in BL Lac objects are difficult to obtain and (2) indirect estimates of σ via the fundamental plane (FP) are highly inaccurate due to the intrinsic scatter of FP relation, as well as to the difficulties in determining the other observables in the FP.

In Figures 9 and 10 we therefore plot the black hole mass versus radio power using the estimates of Falomo et al. (2003). In Figure 9 we use the observed total radio power, as measured at 325 MHz. In Figure 10 we use the core power at 1.4 GHz: in the left panel we plot the observational data; in the right one we consider the debeamed core luminosity, adopting a Lorentz factor $\Gamma = 1/\sin\theta$. Since the intrinsic core luminosity correlates with the total power, we expect similar behaviors in Figures 9 and 10 (*right*).

Neither the total nor the core radio power (corrected and uncorrected) seem to be good indicators of the black hole mass, as the same BH mass is found in objects with radio power more than 2 orders of magnitude apart. Although weak, a trend of larger $M_{\rm BH}$

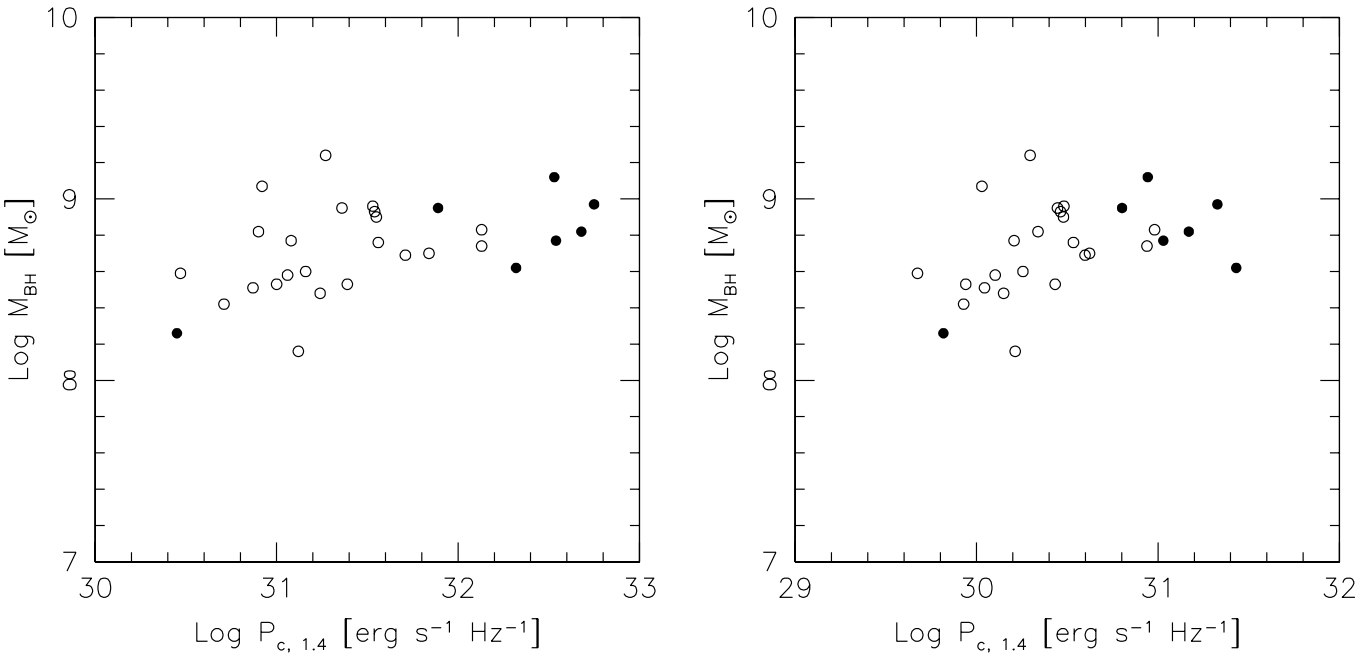


FIG. 10.—BH mass vs. core radio power at 1.4 GHz. *Left*: Observed quantities; *right*: core luminosity debeamed assuming $\Gamma = 1/\sin\theta$. Filled and open symbols represent HBL and LBL, respectively.

TABLE 8
CORRELATION COEFFICIENT FOR BH MASS-RADIO POWER

Radio Power (1)	r_z (2)	$r_{\mathrm{no}\,z}$ (3)	P_{null} (4)
Extended	0.43	0.42	0.011
Core, observed	0.45	0.41	0.014
Core, debeamed with $\Gamma = 1/\theta$	0.42	0.38	0.021

for more powerful radio sources is however present; we also note that the corrected nuclear powers are spread over a narrow range, so that any possible correlation becomes harder to reveal. We plan in the near future to add lower power sources to the BL Lac objects to obtain a larger range.

We report in Table 8 the correlation coefficients for the present sample, describing the significance of the trends visible in the various plots. Since both the radio power and the black hole mass (estimated from host luminosity) include a dependence on redshift, we give in column (3) also the coefficient corrected against z and the corresponding probability of the null hypothesis in column (4). Since this probability is relatively low, it is likely that a correlation between BH mass and radio power is actually present. The large scatter in the correlation, however, suggests that black hole mass alone is not a critical parameter for the emitted radio power in nearby BL Lac objects.

4.2. *Radio and Optical Nuclear Luminosity*

Chiaberge et al. (1999) have exploited *HST* and radio data to discuss the physical properties of nuclei of low-power radio galaxies, finding a linear correlation between optical and radio luminosity. This correlation is interpreted in terms of a common non thermal origin. Hardcastle & Worrall (2000) have studied the nuclei of 3CRR radio galaxies with similar tools, concluding that the emission is jet related and that their properties are related to those of BL Lac objects. Our high-quality radio data and the optical *HST* results (Urry et al. 2000; Falomo et al. 2000) allow us to extend this line of research, moving from the observational properties found in our sample of low-redshift BL Lac objects. We present in Figure 11 the comparison between optical and radio core luminosity for BL Lac objects, together with the correlation found by Chiaberge et al. (1999) for FR I nuclei.

The objects in the present sample span almost three orders of magnitude in observed radio core luminosity and the optical core luminosity increases linearly with it over this interval (Fig. 11, *left*). A strong correlation ($P > 99.99\%$) between optical and radio core luminosity emerges clearly. The flux densities correlate as well as the powers, confirming that this is not an artifact introduced by the common dependence on the luminosity distance (see also the discussion on correlation between intrinsic luminosities in Feretti et al. 1984; Feigelson & Berg 1983). We show here the luminosities only for the sake of homogeneity in the comparison with Chiaberge et al. (1999). This correlation supports the suggestion that, as in FR I radio galaxies, the emission in the two wave bands is ascribed to the same non thermal process, with negligible contribution from, e.g., a thermal disk. However, the optical cores of BL Lac objects are about two magnitudes brighter than those of FR I galaxies with the same core radio luminosity. Notice that we are plotting here *observed* values, i.e., quantities that are affected by beaming. While it is interesting to note that this keeps the correlation tight, we argue that this may be responsible for the optical offset observed for BL Lac objects. Chiaberge et al. (2000) obtained a similar result from the BL Lac objects in the Slew survey, while the LBLs of the 1 Jy sample are less displaced from the correlation than our objects.

In the right panel, we show the luminosities as corrected for the derived Doppler factor. We assume for the optical emission a spectral index $\alpha_O = 1$ (Falomo et al. 1994) and for the radio core $\alpha_R = 0.0$ (Table 6). We also recalculate the luminosities in the hypothesis of a viewing angle of 60°, which is the average angle expected for the population of FR I radio galaxies used

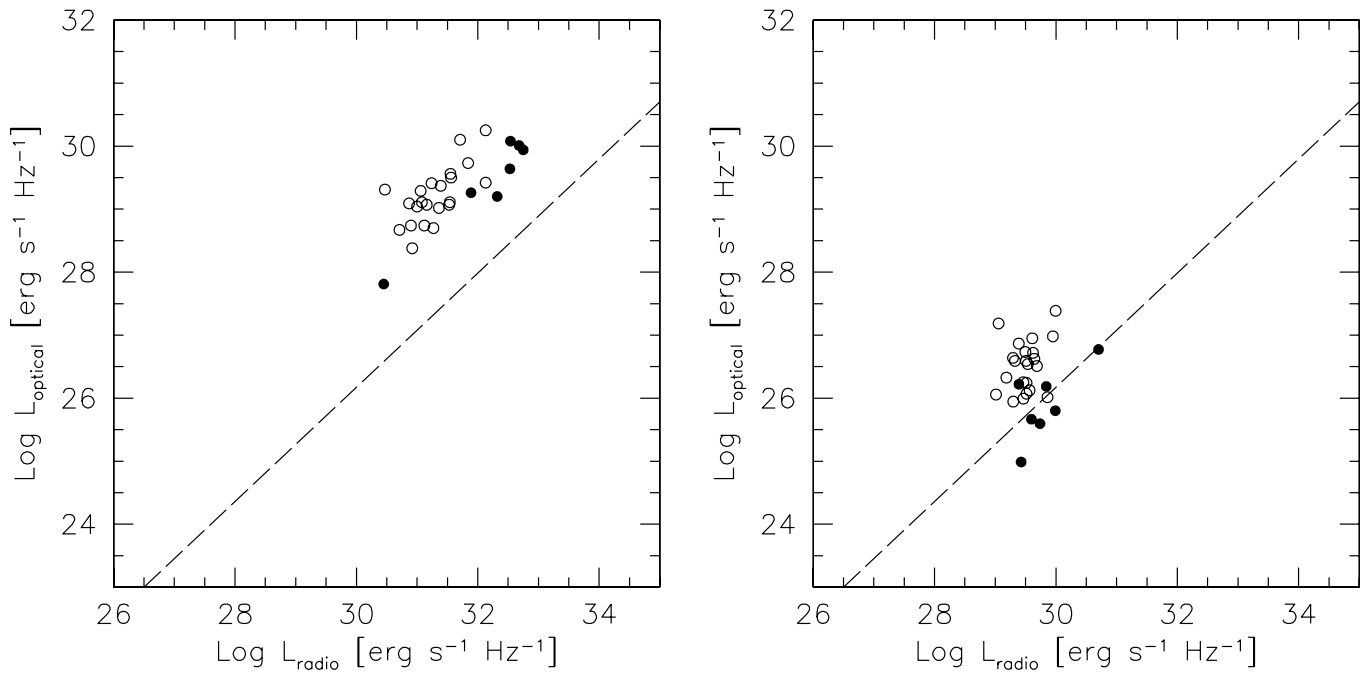


FIG. 11.—Optical vs. radio core power diagram for BL Lac objects in the present sample. Open symbols are HBLs; filled symbols are LBLs. The dashed line shows the radio-optical correlation for cores of FR I radio galaxies (Chiaberge et al. 1999). *Left*: Observed luminosities; *right*: luminosities corrected for Doppler beaming, in the case of a viewing angle of 60° and assuming $\alpha_O = 1$ and $\alpha_R = 0.0$ (see § 4.2).

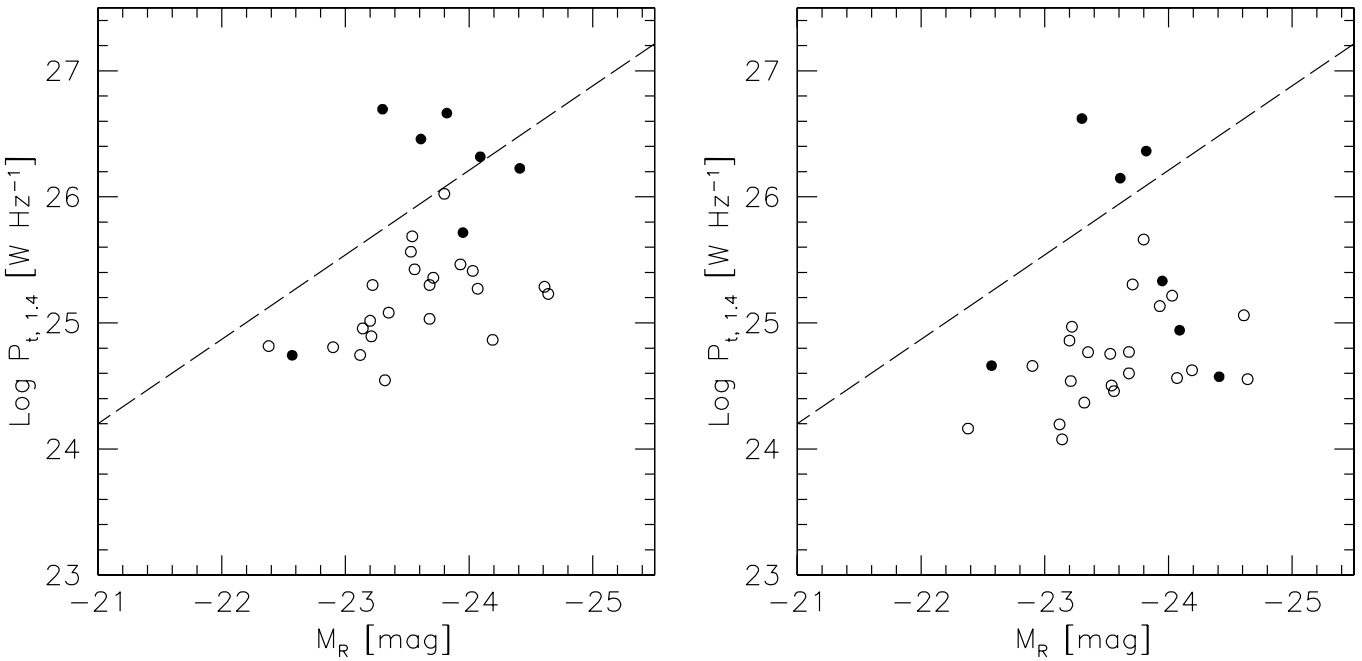


FIG. 12.—Ledlow & Owen diagram; *left*: observed; *right*: intrinsic. For ease of comparison with similar plots, we have rescaled our data to $H_0 = 50$ km s^{-1} Mpc^{-1} and $q_0 = 0$. The quantities on the x- and y-axis (host magnitude and total radio power) are a measure of the BH mass and accretion rate, respectively. The dashed line corresponds to $L_{\rm jet} \sim 0.015 L_{\rm Edd}$ (Ghisellini & Celotti 2001). The three objects that remain above the line are 0521−365, 0829+046, and 2200+420. Filled and open circles represent LBL and HBL, respectively.

by Chiaberge et al. (1999) to derive the correlation. As an effect of debeaming, all the points move to lower radio and optical luminosities and approach the correlation for radio galaxies, with some scatter. This makes a strong point in favor of a common nature of BL Lac objects and FR I radio galaxy cores. The little scatter left in the debeamed values and in particular the systematic offset for HBL sources, although little, could be suggestive of some finer detail. For example, a two velocity jet (fast spine and slower external layer, with different weights in LBL and HBL) is a plausible solution that accounts also for other observational properties, such as limb brightening of jets (Giroletti et al. 2004b).

Finally, we note that it would have been possible to use our VLBI data to calculate parsec-scale radio luminosities. We have not done this for the sake of homogeneity in the comparison with FR I galaxies. However, it is interesting to reconsider the subject once we have parsec-scale data for a large unbiased sample of low-power radio galaxies, such as the Bologna Complete Sample (Giovannini et al. 2005, M. Giroletti et al. 2006, in preparation).

4.3. *Ledlow & Owen Diagram*

Figure 12 shows the distribution of the objects belonging to the present sample in the Ledlow & Owen diagram, in which the dashed line separates FR I and FR II radio galaxies (Ledlow & Owen 1996). When we consider the observed values (*left*), about 20% of our nearby BL Lac objects fall in the FR II domain or across the transition region. However, the core fraction of the total luminosity is still significant at 1.4 GHz, so we have to separate the core and extended radio luminosity and debeam the former. We show the intrinsic quantities that we derive in this way in the right panel: most objects move deep into the region typical of FR I radio galaxies, leaving only three sources in the FR II and transition region: 0521−365, 0829+046, and 2200+420 (all LBLs).

In order to discuss the implication of this distribution in the Ledlow & Owen diagram, we consider again the relationship between optical magnitude of the host and BH mass, as well as the one between radio power and total jet kinetic power (Willott et al. 1999). We can then interpret the diagram in terms of BH mass and jet power: for a given $M_{\rm BH}$, FR II galaxies have jets of total power above a certain value, which becomes larger for more massive black holes. In other words, there is a critical ratio between jet power and black hole mass that divides FR I and FR II radio galaxies. Our sources seem to produce radio jets of low kinetic power with respect to FSRQ and FR II radio galaxies with similar BH masses.

One can speculate about the interpretation of the FR I/FR II dichotomy; for example, Willott et al. (1999) have related the total radio power to the narrow emission-line luminosity, which is directly produced by photoionization from the nuclear accreting radiation. Using these correlations, one could estimate accretion rates for FR I galaxies and BL Lac objects and speculate that they are sub-Eddington systems with subcritical accretion rates (Ghisellini & Celotti 2001). Unfortunately, line luminosity is generally not available for sources in our sample and the validity of such assumptions cannot be established.

4.4. *The Fundamental Plane of BH Activity*

A correlation between X-ray and radio emission is expected if there is a fundamental connection between accretion flows and jet activity. Merloni et al. (2003) have considered a large sample of objects (AGNs and X-ray binaries) powered by super– massive black holes (SMBHs) as well as galactic BHs. From the study of their radio core luminosity, 2–10 keV X-ray luminosity, and BH mass, a fundamental plane (FP) of BH activity is found. However, BL Lac objects have been excluded from this study, since Doppler boosting of the jet emission is expected to spoil the correlation.

In Figure 13 (*left*), we show the position of our nearby BL Lac objects in the projection of the FP, as obtained from the observed (i.e., Doppler boosted) values: it is readily visible that the

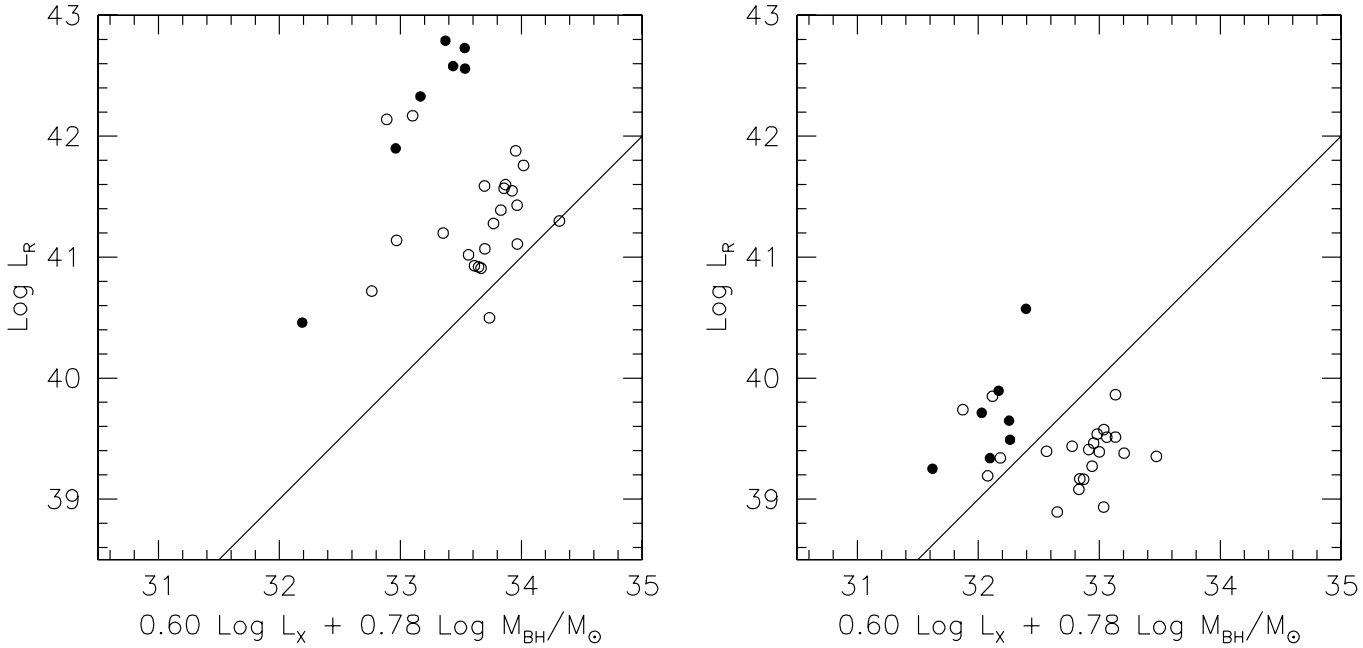


FIG. 13.—"Edge-on" view of the fundamental plane of BH activity; the line shows the best fit to the sample of SMBH and galactic BHs studied by Merloni et al. (2003). *Left*: Observed quantities; *right*: corrected for Doppler boosting and recalculated for a mean viewing angle of 60°. Filled and open circles represent LBL and HBL, respectively.

observed radio luminosities are well above the correlation. From the derived intrinsic debeamed values,[7] we then plot in the right-hand panel the new L_R versus $0.60 \log L_X + 0.78 \log M_{BH}\ M_\odot^{-1}$, recalculated in the case of a viewing angle of 60° (which is the average angle for the objects used to derive the correlation). The corrected data seem to cluster around the FP relation, albeit with a significant scatter in the points. Although no systematic general offset is found, we note that LBLs (*filled circles*) lie above/left of the correlation, while HBLs are preferentially found below/right of it.

It is thus interesting that AGNs with radio jets, like our BL Lac objects, follow the same relation of the bulk of SMBHs and galactic BHs. On one hand, this finding could support the existence of the general fundamental connection between accretion flows and jet activity (Merloni et al. 2003; Falcke et al. 2004). In this case, the possible offset between LBLs and HBLs could be suggestive of a possible refinement of the proposed models, requiring more powerful radio jets in LBLs or an accreting process that is more radiatively efficient in HBLs. On the other hand, it has been suggested that the FP relation is actually an artifact due to the flux-limited nature of the sample considered (Bregman 2005). Once the Doppler-boosting dependence has been removed, a common dependence on distance in the plotted quantities could become apparent. Since our sample is volume limited ($z < 0.2$), rather than flux limited, we should, however, be free from this bias: we have radio and X-ray fluxes spanning 3 orders of magnitude each (radio fluxes between 7 mJy and 5 Jy, and X-ray 2–10 keV fluxes between 0.4 and 240 ergs $cm^{-2}\ s^{-1}$).

5. CONCLUSIONS

We have presented new high-resolution images for 9 BL Lac objects. Parsec-scale images reveal an almost ubiquitous presence of one-sided jets. Under the assumption of intrinsically symmetric jets, this provides evidence for relativistic velocities in the parsec-scale region of jets. This result supports the previous findings on the same sample (Giroletti et al. 2004a), and we conclude that the Lorentz factors in the sample cluster around $\Gamma \sim 4$, mainly on the basis of the core dominance argument. In the best studied sources, thanks to the short baselines provided by the MERLIN, we examine the jet out to several hundred parsecs and still find no evidence of counterjets. On kiloparsec scales, the structure of 1728+502 remains aligned with the inner region direction, while 1215+303 and Mrk 421 reveal a symmetric structure without a clear connection with the parsec-scale jet. In Mrk 421 we have evidence of limb brightening of the jet, from the very inner jet region (~2 mas from the core) out to ~30 mas. This result, similar to what is found in the other TeV source Mrk 501 (Giroletti et al. 2004b), is of great importance in the development of jet launch models and the study of the jet/environment interaction.

X-ray fluxes and high-resolution optical data available for our whole sample of 29 nearby BL Lac objects allow us to perform a multiwavelength analysis. In particular, by resolving the host galaxy and separating the nonthermal core, we have been able to discuss the physical properties of the BL Lac phenomenon. Given the distance-limited nature of the present sample, we are confident of the robustness of our results, which we summarize as follows:

1. There is a significant correlation between the mass of the central SMBH and the radio luminosity, both nuclear and extended, independent of any common distance dependence. However, there is a large scatter in the correlation, so that radio luminosity alone cannot be taken as an indicator of the BH mass.

2. Radio and optical nuclear luminosities (and fluxes) show a strong correlation, indicating a common origin for the emission at both wavelengths, i.e., nonthermal synchrotron radiation. Moreover, if we debeam the observed luminosities, the cores follow with little scatter the same correlation found for low-power radio galaxies by Chiaberge et al. (1999), in strong support of the unification of BL Lac objects and FR I galaxies based on orientation.

3. Still in support of the BL Lac/FR I unification, our sources lie below the dividing line in the Ledlow & Owen diagram; for

[7] The X-rays luminosities have been debeamed assuming a spectral index $\alpha_X = 0.7$.

any given M_{BH}, low-redshift BL Lac objects have lower radio power than FR II radio galaxies of similar M_{BH}.

4. The radio and X-ray luminosities do not follow the fundamental plane of BH activity found for other supermassive and galactic BHs, clearly because of the relevant Doppler boosting of the jet. When we consider debeamed quantities, the FP relation becomes quite well-reproduced, although some overall scatter and an LBL-HBL offset appear.

We thank an anonymous referee for a constructive report that improved the clarity of the paper. This research has made use of the NASA/IPAC Extragalactic Database (NED), which is operated by the Jet Propulsion Laboratory, Caltech, under contract with NASA and of NASA's Astrophysics Data System (ADS) Bibliographic Services. The European VLBI Network is a joint facility of European, Chinese, South African, and other radio astronomy institutes funded by their national research councils. MERLIN is a National Facility operated by the University of Manchester at Jodrell Bank Observatory on behalf of PPARC. The National Radio Astronomy Observatory is a facility of the National Science Foundation, operated under cooperative agreement by Associated Universities, Inc. This material is based on work supported by the Italian Ministry for University and Research (MIUR) under grant COFIN 2003-02-7534.

REFERENCES

Aharonian, F., et al. 2002, A&A, 384, L23
Baum, S. A., Zirbel, E. L., & O'Dea, C. P. 1995, ApJ, 451, 88
Becker, R. H., White, R. L., & Helfand, D. J. 1995, ApJ, 450, 559
Bregman, J. N. 2005, ApJL, submitted (astro-ph/0511368)
Cassaro, P., Stanghellini, C., Dallacasa, D., Bondi, M., & Zappalà, R. A. 2002, A&A, 381, 378
Chiaberge, M., Capetti, A., & Celotti, A. 1999, A&A, 349, 77
Chiaberge, M., Celotti, A., Capetti, A., & Ghisellini, G. 2000, A&A, 358, 104
Denn, G. R., Mutel, R. L., & Marscher, A. P. 2000, ApJS, 129, 61
De Young, D. S. 1993, ApJ, 405, L13
Donato, D., Ghisellini, G., Tagliaferri, G., & Fossati, G. 2001, A&A, 375, 739
Donato, D., Sambruna, R. M., & Gliozzi, M. 2005, A&A, 433, 1163
Falcke, H., Koerding, E., & Markoff, S. 2004, A&A, 414, 895
Falomo, R., Carangelo, N., & Treves, A. 2003, MNRAS, 343, 505
Falomo, R., Scarpa, R., & Bersanelli, M. 1994, ApJS, 93, 125
Falomo, R., Scarpa, R., Treves, A., & Urry, C. M. 2000, ApJ, 542, 731
Feigelson, E. D., & Berg, C. J. 1983, ApJ, 269, 400
Feretti, L., Giovannini, G., Gregorini, L., Parma, P., & Zamorani, G. 1984, A&A, 139, 55
Ferrarese, L., & Merritt, D. 2000, ApJ, 539, L9
Gebhardt, K., et al. 2000, ApJ, 539, L13
Ghisellini, G., & Celotti, A. 2001, A&A, 379, L1
Ghisellini, G., Tavecchio, F., & Chiaberge, M. 2005, A&A, 432, 401
Giovannini, G., Cotton, W. D., Feretti, L., Lara, L., & Venturi, T. 1999, Mem. Soc. Astron. Italiana, 70, 161
Giovannini, G., Taylor, G. B., Feretti, L., Cotton, W. D., Lara, L., & Venturi, T. 2005, ApJ, 618, 635
Giroletti, M., Giovannini, G., Taylor, G. B., & Falomo, R. 2004a, ApJ, 613, 752
———. 2005, in ASP Conf. Ser. 340, Future Directions in High Resolution Astronomy: The 10th Anniversary of the VLBA, ed. J. Romney & M. Reid (San Francisco: ASP), 62
Giroletti, M., et al. 2004b, ApJ, 600, 127
Hardcastle, M. J., & Worrall, D. M. 2000, MNRAS, 314, 359
Horan, D., et al. 2002, ApJ, 571, 753
Kollgaard, R. I., Gabuzda, D. C., & Feigelson, E. D. 1996, ApJ, 460, 174
Kormendy, J., & Gebhardt, K. 2001, in AIP Conf. Proc. 586, 20th Texas Symposium on Relativistic Astrophysics, ed. J. C. Wheeler & H. Martel (Melville: AIP), 363
Ledlow, M. J., & Owen, F. N. 1996, AJ, 112, 9
Magorrian, J., et al. 1998, AJ, 115, 2285
Merloni, A., Heinz, S., & di Matteo, T. 2003, MNRAS, 345, 1057
Morris, S. L., Stocke, J. T., Gioia, I. M., Schild, R. E., Wolter, A., Maccacaro, T., & della Ceca, R. 1991, ApJ, 380, 49
Perlman, E. S., et al. 1996, ApJS, 104, 251
Piccinotti, G., Mushotzky, R. F., Boldt, E. A., Holt, S. S., Marshall, F. E., Serlemitsos, P. J., & Shafer, R. A. 1982, ApJ, 253, 485
Piner, B. G., & Edwards, P. G. 2004, ApJ, 600, 115
———. 2005, ApJ, 622, 168
Punch, M., et al. 1992, Nature, 358, 477
Rector, T. A., Gabuzda, D. C., & Stocke, J. T. 2003, AJ, 125, 1060
Rector, T. A., Stocke, J. T., Perlman, E. S., Morris, S. L., & Gioia, I. M. 2000, AJ, 120, 1626
Scarpa, R., Urry, C. M., Falomo, R., Pesce, J. E., & Treves, A. 2000a, ApJ, 532, 740
Schachter, J. F., et al. 1993, ApJ, 412, 541
Stickel, M., Fried, J. W., Kuehr, H., Padovani, P., & Urry, C. M. 1991, ApJ, 374, 431
Urry, C. M., Scarpa, R., O'Dowd, M., Falomo, R., Pesce, J. E., & Treves, A. 2000, ApJ, 532, 816
Willott, C. J., Rawlings, S., Blundell, K. M., & Lacy, M. 1999, MNRAS, 309, 1017